Comunicações Geológicas

Comunicações Geológicas (2025) 112, 1, 21-34
ISSN: 0873-948X; **e-ISSN:** 1647-581X

Zeolites and associated minerals as indicators of post-magmatic hydrothermal alteration in Mesozoic tholeiitic basalts in Northeastern Brazil

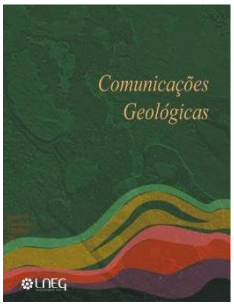

Zeolitas e minerais associados como indicadores de alteração hidrotermal pós-magmática em basaltos toleíticos mesozoicos no Nordeste do Brasil

L. M. Lima de Araújo[1], F. C. J. Vilalva[1,2*], R. F. Souza[2,3], A. Bustamante[4], L. Cunha de Souza[2]

DOI: https://doi.org/10.34637/6akm-3g23
Recebido em 30/10/2024 / Aceite em 06/06/2025
Publicado online em junho de 2025

Artigo original
Original article

Abstract: In northeastern Brazil, tholeiitic basalts and microgabbros from the Rio Ceará-Mirim dike swarm and Serra do Cuó basaltic flow experienced post-magmatic hydrothermal alteration, forming secondary minerals that replaced magmatic phases and filled amygdules. Petrographic, X-ray diffraction, thermogravimetric, and chemical analyses identified laumontite, quartz, and calcite as the dominant amygdule minerals in the Rio Ceará-Mirim dikes, formed at temperatures < 150 °C (Stage II) following an earlier low to moderate-temperature (< 150 – 200 ºC) alteration phase (Stage I). In the Serra do Cuó basalts, polymineralic amygdule formation began with mafic phyllosilicates (from < 150 to ~200 °C, Stage I) and proceeded to Ca-Na zeolites (~250 °C, Stage II). These assemblages reflect fluid composition changes due to primary mineral destabilization by heated meteoric fluids. Results indicate fluid composition, rather than temperature, as the primary control on mineral variability, highlighting the role of host-rock chemistry in hydrothermal alteration.

Keywords: Rio Ceará-Mirim Dike Swarm, Serra do Cuó basalts, Borborema Province, meteoric fluids, amygdules.

Resumo: No nordeste do Brasil, basaltos toleíticos e microgabros do enxame de diques Rio Ceará-Mirim e do derrame basáltico Serra do Cuó passaram por alteração hidrotermal pós-magmática, resultando na formação de minerais secundários que substituíram fases magmáticas e preencheram amígdalas. Análises petrográficas, difracção de raios X, análises termogravimétricas e químicas identificaram laumontite, quartzo e calcite como os principais minerais nas amígdalas dos diques Rio Ceará-Mirim, formados a temperaturas < 150 °C (Estágio II), após uma fase prévia de alteração a temperaturas baixas a moderadas (< 150 – 200 °C Estágio I). Nos basaltos Serra do Cuó, a formação de amígdalas poliminerálicas iniciou-se com filossilicatos máficos (de temperaturas < 150 °C até ~200 °C, Estágio I), e prosseguiu com zeolitas cálcio-sódicas (~250 °C, Estágio II). Estas associações refletem mudanças na composição dos fluidos, decorrentes da destabilização dos minerais primários por fluidos meteóricos aquecidos. Os resultados indicam que a composição do fluido, mais do que a temperatura, é o principal fator controlador da variabilidade mineral, sublinhando o papel da química da rocha hospedeira na alteração hidrotermal.

Palavras-Chave: Enxame de Diques no Rio Ceará-Mirim, basaltos da Serra do Cuó, Província Borborema, fluidos meteóricos, amígdalas.

[1] Programa de Pós-Graduação em Geodinâmica e Geofísica (PPGG), Universidade Federal do Rio Grande do Norte (UFRN), Natal, RN, Brazil.
[2] Departamento de Geologia, Centro de Ciências Exatas e da Terra, Universidade Federal do Rio Grande do Norte (UFRN). R. das Engenharias, s/n – Campus Central, 59078-970, Natal, RN, Brazil.
[3] Programa Regional de Pós-Graduação em Desenvolvimento e Meio Ambiente (PRODEMA), Universidade Federal do Rio Grande do Norte (UFRN), Natal, RN, Brazil.
[4] Departamento de Geologia, Centro de Tecnologia e Geociências, Universidade Federal de Pernambuco (UFPE). Av. da Arquitetura, s/n - Cidade Universitária, 50740-540, Recife, PE, Brazil.

* Corresponding author / Autor correspondente: frederico.vilalva@ufrn.br

1. Introduction

Basaltic rocks commonly experience hydrothermal alteration through hot aqueous or meteoric fluids, resulting in secondary minerals like chalcedony, clays, zeolites, and carbonates that replace magmatic phases and fill amygdules, vugs, and veins (Kristmannsdóttir, 1979; Eggleton *et al*., 1987; Markússon and Stefánsson, 2011; Walker, 1960). The formation of these minerals depends on the composition of the basalt and the temperature, pressure, and pH of interacting fluids (Kristmannsdóttir and Tomasson, 1978; Duarte *et al*., 2009; Kónya and Szakáll, 2011; Kousehlar *et al*., 2012; Mattioli *et al*., 2016). Examining these secondary mineral assemblages in basaltic rocks provides insights into their thermal history, alteration processes, and fluid evolution (Robert, 2001; Mattioli *et al*., 2016).

Northeastern Brazil hosts significant continental tholeiitic magmatism linked to the breakup of Gondwana during the Mesozoic. This activity, is marked by dike swarms in Precambrian rocks and small volcanic flows, and has two major episodes: the Rio Ceará-Mirim dike swarm (~130 Ma) and the Serra do Cuó basaltic flow (93 – 99 Ma) (Fig. 1; Sial, 1978; Bellieni *et al*., 1992; Mizusaki *et al*., 2002; Souza *et al*., 2003; Hollanda *et al*., 2006; Ngonge *et al*., 2016; Hollanda *et al*., 2019; Macêdo Fillho *et al*., 2025). Despite thorough petrographic, geochemical, isotopic, and geochronological studies, detailed mineralogical descriptions of secondary mineral paragenesis filling vesicles and replacing

primary minerals in these rocks are limited. Thus, the hydrothermal and post-magmatic processes affecting these rocks remain insufficiently understood.

This study aims to characterize zeolites and other secondary minerals in amygdules from samples of the Rio Ceará-Mirim dike swarm and Serra do Cuó basaltic flow. Using petrography, X-ray diffraction, thermogravimetry, and in situ chemical analyses, we identify distinct mineral assemblages and examine how the basalt composition and fluid chemistry influenced this mineral diversity.

2. Geological Setting

The Borborema Province in northeast Brazil is a key component of West Gondwana, formed by the convergence of the West African and São Francisco-Congo cratons during the Late Neoproterozoic Brazilian/Pan-African Orogeny. This province has a complex geological framework, including an Archean-Neoproterozoic basement with metamorphosed supracrustal sequences and numerous Neoproterozoic plutons (Fig. 1b; Almeida *et al*., 1981; Arthaud *et al*., 2008; Van Schmus *et al*., 2008; Souza *et al*., 2016; Caxito *et al*., 2020). These units intersect with large-scale, high-temperature shear zones (Vauchez *et al*., 1995; Neves *et al*., 2021). Additionally, the Cretaceous opening of the Equatorial Atlantic triggered extensive rifting and tholeiitic magmatism (Bellieni *et al*., 1992; Mizusaki *et al*., 2002; Hollanda *et al*., 2006; Ngonge *et al*., 2016; Hollanda *et al*., 2019).

This tholeiitic magmatism occurred in four main phases during the Mesozoic. The earliest, represented by the Rio Ceará-Mirim

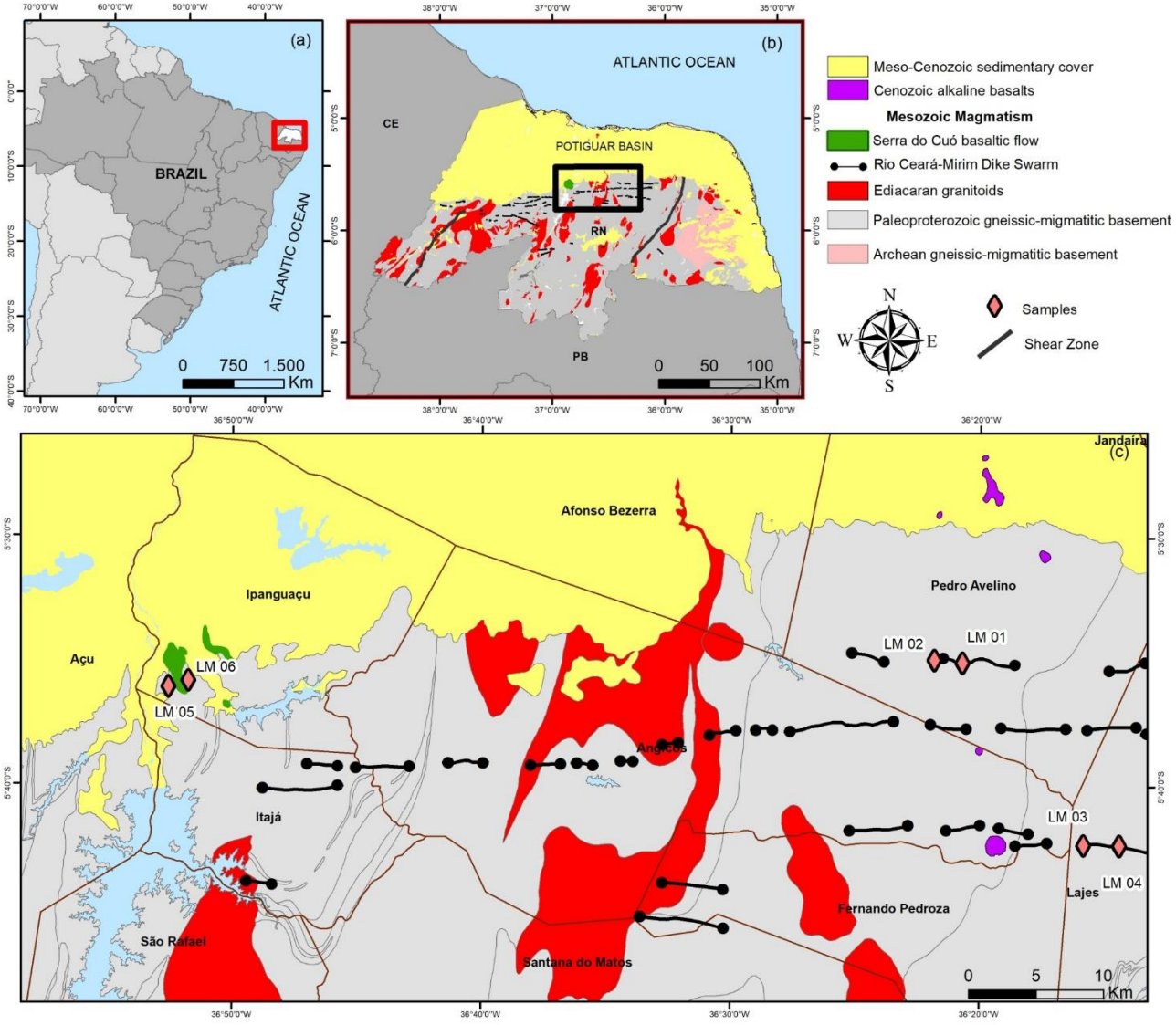

Figure 1. Maps showing the location of the study area. (a) Map of South America indicating the location of the state of Rio Grande do Norte, Brazil; (b) simplified geological map of Rio Grande do Norte in northeastern Brazil; (c) geological sketch of the study area in Rio Grande do Norte (RN) between the cities of Lajes and Açu, highlighting the outcrops of the Rio Ceará-Mirim dike swarm and the Serra do Cuó basaltic flow, as well as the locations of the studied samples. Modified from Angelim *et al.* (2006). The neighboring states of Ceará (CE) and Paraíba (PB) are also shown.

Figura 1. Mapas mostrando a localização da área de estudo. (a) Mapa da América do Sul indicando a localização do estado do Rio Grande do Norte, Brasil; (b) mapa geológico simplificado do Rio Grande do Norte, no nordeste do Brasil; (c) esboço geológico da área de estudo no Rio Grande do Norte (RN), entre as cidades de Lajes e Açu, destacando os afloramentos do enxame de diques Rio Ceará-Mirim e do derrame basáltico Serra do Cuó, bem como as localizações das amostras estudadas. Modificado de Angelim *et al.* (2006). Também são mostrados os estados vizinhos Ceará (CE) e Paraíba (PB).

dike swarm (CMD), consists of diabase and basalt, while the latest phase includes minor alkaline basaltic flows from the Serra do Cuó basaltic flow (SCB) (Figs. 1b, c). The CMD is recognized as part of the Equatorial Atlantic Magmatic Province (EQUAMP), a major Cretaceous Large Igneous Province (LIP) (Hollanda *et al*., 2019). The CMD comprises mafic dikes that extend up to 400 km, range from 1 to 190 m in width, and trend east-west, with a southwest shift near 38°W (Ngonge *et al*., 2016; Hollanda *et al*., 2019). These dikes, primarily subalkaline tholeiitic basalts to basaltic trachyandesites, date between 145 and 115 Ma (K/Ar methods) and 132 – 118 Ma ($^{40}Ar/^{39}Ar$) (Bellieni *et al*., 1992; Mizusaki *et al*., 2002; Souza *et al*., 2003; Ngonge *et al*., 2016). The CMD dikes examined here are situated between Açu and Lajes (Rio Grande do Norte State, Brazil) in north-central Borborema (Figs. 1b, c).

The SCB comprises small volcanic flows near Ipanguaçu (Rio Grande do Norte), marking the boundary between the Borborema basement and the Cretaceous Potiguar Rift Basin, and extending into north-central Borborema (Figs. 1b, c). These fine- to medium-grained basalts and trachybasalts exhibit alkaline to tholeiitic affinities (Fig. 2). K-Ar dating places SCB activity at ~90 Ma, while $^{40}Ar/^{39}Ar$ dating on plagioclase yields an age of 93 ± 1 Ma (Souza *et al*., 2003). Slightly older ages (~98 Ma) were reported by Araújo *et al*. (2001) for the same magmatism, whereas recent whole-rock $^{40}Ar/^{39}Ar$ dating indicates a minimum crystallization age of 99 ± 1 Ma (Macêdo Filho *et al*., 2025). Mizusaki *et al*. (2002) linked SCB with the formation of the youngest oceanic crust along the Brazilian eastern margin, coinciding with the final separation of South America and Africa. Macêdo Filho *et al*. (2025) recently suggested this magmatism may be related to changes in South America drift pattern and possible interactions between asthenospheric and lithospheric processes during the Cenomanian.

3. Materials and methods

Twenty samples of CMD and SCB basalts and microgabbros were collected from six representative outcrops in the north-central Borborema Province, between Açu and Lajes, Rio Grande do Norte (Fig. 1b, c; Tab. 1). Each sample was examined under a polarizing microscope, and 1 cm cubes with prominent millimeter to centimeter-sized amygdules were prepared for stereomicroscopic observation of the cavity infillings.

Scanning electron microscopy (SEM) was used to analyze the morphology of cavity infillings across three laboratories: (1) the Laboratório de Caracterização de Minerais e Materiais (LACAMM) at the Instituto Federal de Educação, Ciência e

Table 1. Selected samples of amygdaloidal basalts and microgabbros from the Rio Ceará-Mirim dike swarm and the Serra do Cuó basaltic flow. UTM coordinates were measured using the SIRGAS 2000 datum; all coordinates fall within zone 24S.

Tabela 1. Amostras selecionadas de basalto amigdaloidal e microgabro do enxame de diques Rio Ceará-Mirim e do derrame basáltico Serra do Cuó. As coordenadas UTM foram medidas usando o datum SIRGAS 2000; todas as coordenadas estão na zona 24S.

Sample	Magmatism	N	E
LM 01.1, LM 01.2	Rio Ceará-Mirim	792601	9382424
LM 02	Rio Ceará-Mirim	792277	9382360
LM 03.2; LM 03.4	Rio Ceará-Mirim	804933	9368626
LM 04.2	Rio Ceará-Mirim	805550	9368536
LM 05.2; LM 05.3	Serra do Cuó	736417	9380278
LM 06.2; LM 06.3	Serra do Cuó	736417	9380682

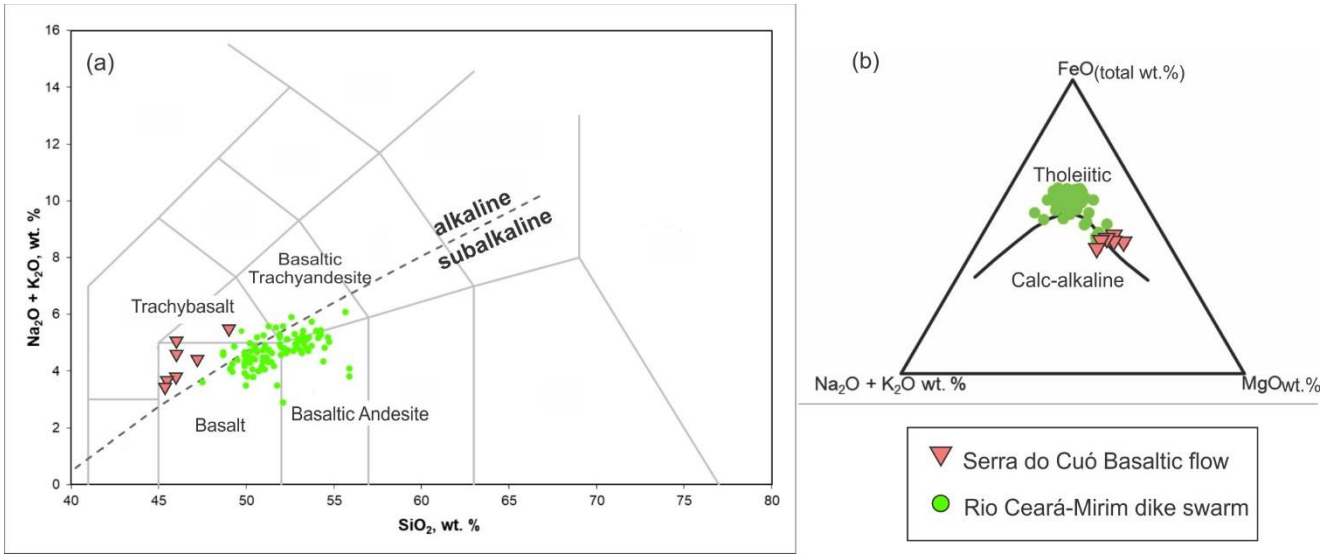

Figure 2. Major whole-rock classification diagrams for the Mesozoic tholeiitic basalts and microgabbros of the Rio Ceará-Mirim dike swarm and Serra do Cuó basaltic flow in northeastern Brazil. (a) Total Alkali-Silica (TAS) diagram from Le Bas *et al*. (1986), with the boundary between alkaline and subalkaline series from Irvine and Baragar (1971); (b) Total Alkalis-FeO-MgO (wt.%) ternary plot (AFM) from Irvine and Baragar (1971). Data sources: Sial (1978); Bellieni *et al*. (1992); Hollanda *et al*. (2006); Ngonge *et al*. (2016).

Figura 2. Diagramas de classificação de rocha total para basaltos toleíticos e microgabros mesozóicos do enxame de diques Rio Ceará-Mirim e do derrame basáltico Serra do Cuó no nordeste do Brasil. (a) Diagrama Total Alcalis-Sílica (TAS) de Le Bas *et al.* (1986), com a divisão entre séries alcalinas e subalcalinas de Irvine e Baragar (1971); (b) diagrama ternário Total Alcalis-FeO-MgO (em %) (AFM) de Irvine e Baragar (1971). Fontes de dados: Sial (1978); Bellieni *et al*. (1992); Hollanda *et al.* (2006); Ngonge *et al*. (2016).

Tecnologia do Rio Grande do Norte (IFRN), equipped with a TESCAN VEGA3 SEM coupled to an Oxford Instruments X-act energy-dispersive X-ray spectroscopy (EDS) microanalysis system; (2) the Laboratório de Dispositivos e Nanoestruturas (LDN) at the Universidade Federal de Pernambuco (UFPE), using a JEOL JSM-6460 SEM with an Oxford Instruments wavelength-dispersive X-ray spectroscopy (WDS) system; and (3) the Laboratório de Peneiras Moleculares (LABPEMOL) at the Universidade Federal do Rio Grande do Norte (UFRN), equipped with a TESCAN MIRA 4 SEM paired with an Oxford Instruments Ultim Max EDS system.

Chemical compositions of secondary minerals within cavities were measured at LDN-UFPE under the following conditions: 20 kV acceleration voltage, 20 nA beam current, 1 µm beam diameter, ~50 s acquisition time, and 8 mm working distance. Key spectral lines, standards, and associated uncertainties (2σ) included: SiKα (quartz, ± 0.4), AlKα (corundum, ± 0.2), FeKα (metallic iron, ± 0.4), MgKα (periclase, ± 0.3), CaKα (wollastonite, ± 0.2), NaKα (amelia albite, ± 0.2), and KKα (MAD-10 feldspar, ± 0.2).

Zeolite mineral compositions were recalculated by subtracting H_2O content, as determined by ideal structural formulae (Coombs *et al*., 1997; Deer *et al*., 2013). Quality checks were applied based on formula balance error (E%) using the method by Passaglia (1970), calculated as E% = [(Al + Fe^{3+}) - Altheor / Altheor] * 100, with Altheor = (Na + K) + 2*(Ca + Mg + Ba + Sr). Positive errors indicate an excess of trivalent cations, while negative errors suggest an excess of exchangeable cations. E values within ±10% were considered reliable (cf., Passaglia, 1970).

Amygdule filling minerals were manually extracted, scraped, and powdered (< 200 mesh) for X-ray diffraction (XRD) and thermogravimetric (TGA) analysis. Limited amygdule volume yielded sufficient powder for XRD in only four samples, analyzed using a Rigaku Miniflex diffractometer at Laboratório de Difração de raios-X, Departamento de Física Teórica e Experimental (DFTE), UFRN. Samples were scanned from 5° to 85° 2θ with a 0.01° step size and Cu Kα radiation. Phase identification employed Crystal Impact Match! Software (v.3.11) and the Crystallography Open Database (COD), with qualitative diffractogram interpretation following Chen (1977).

TGA was conducted at the Laboratório de Propriedades Físicas de Materiais Cerâmicos (LaPFiMC), DFTE/UFRN, using a Shimadzu DTG-60H analyzer. Samples were analyzed under an argon atmosphere, with a 10 °C/min heating rate over a temperature range of 25 – 1000 °C.

4. Results

4.1 Petrographic characterization

4.1.1 Rio Ceará-Mirim dike swarm

The CMD dikes cut through gneissic-migmatitic basement rocks (Fig. 1c) and exhibit textures ranging from fine-grained basalts to medium-grained microgabbros (Figs. 3a, b), varying with dike width. The basalts are mainly porphyritic, while microgabbros show inequigranular, subophitic, and intergranular textures. Primary minerals include clinopyroxenes (32%, diopside, augite, and some pigeonite), Ca-plagioclase (55%), and Fe-Ti oxides (10%), with accessory minerals (3%) like olivine, apatite, biotite, and amphibole (cf., Ngonge *et al*., 2016). The groundmass contains cryptocrystalline material, possibly devitrified glass, with calcite and magnetite particles observed via backscattered electron analysis (Archanjo *et al*., 2002). Secondary minerals, resulting

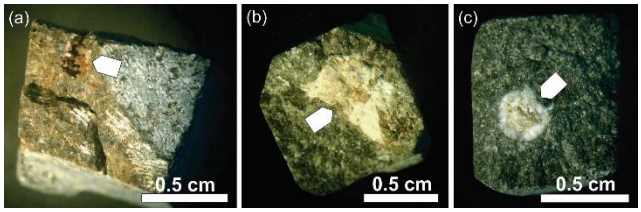

Figure 3. Macroscopic views of amygdules (indicated by white arrows) in basalts and microgabbros from the Rio Ceará-Mirim dike swarm [(a) and (b)] and the Serra do Cuó basaltic flow (c). Samples: (a) LM-01.1, (b) LM-03, and (c) LM-05.2.

Figura 3. Vistas macroscópicas de amígdalas (indicadas por setas brancas) em basaltos e microgabros do enxame de diques Rio Ceará-Mirim [(a) e (b)] e do derrame basáltico Serra do Cuó (c). Amostras: (a) LM-01.1, (b) LM-03 e (c) LM-05.2.

from the alteration of ferromagnesian phases and plagioclase feldspar, include phyllosilicates (predominantly smectite-group minerals and dioctahedral white mica), Fe-oxyhydroxide phases, and carbonate minerals. Amygdules, corresponding to 10 – 20% of the rock volume, are present in both basalts and microgabbros. They vary in shape – typically irregular, elongated, or ellipsoidal, with occasional rounded forms – and range from 0.02 – 0.03 cm in basalts to 1.0 – 2.0 cm in microgabbros (Figs. 3a, b). These amygdules are mostly monomineralic, containing white to orange prismatic or tabular zeolites (hardness < 5; Figs. 4a-c) or granular quartz (Fig. 4e).

Polarizing microscopy shows that zeolite crystals are biaxially negative with low birefringence (~0.012; Figs. 4a-c) and exhibit perfect cleavage along {010} and {110} directions (Fig. 4d). SEM images reveal prismatic, monoclinic forms with cleavage that produces splinters (Figs. 4g-i). Occasionally, amygdules near fracture zones in the host basalt also contain calcite (Fig. 4f).

4.1.2 Serra do Cuó basaltic flow

The SCB samples were collected from the type locality between Ipanguaçu and Açu cities (Fig. 1c). These rocks consist mainly of fine-grained basalts with some medium-grained microgabbros, displaying porphyritic or glomeroporphyritic textures. The primary minerals include olivine (15% phenocrysts), clinopyroxene (25%, mainly augite), Ca-plagioclase (50%), and Fe-Ti oxides (5%). Devitrified, palagonized glass (5%) defines intersertal textures. Secondary minerals, predominantly comprising phyllosilicates (smectite-group minerals, white mica), iddingsite, and Fe-oxyhydroxides, have formed as alteration products of primary mafic silicates, glass, and plagioclase.

Amygdules, comprising 5 – 15% of the SCB rock volume, are rounded and typically under 1 cm in diameter. They are generally polymineralic, showing gradual infilling by secondary minerals that indicate multiple formation phases (Fig. 3c). This process creates mineral zoning, with outer rims featuring colorless to greenish or brown fine-grained aggregates with resinous to waxy luster and platy or botryoidal textures. Central zones are filled with either (1) prismatic colorless crystals altered to an orange-brown dull material with low birefringence or (2) bladed and fibrous white to brownish crystals, accompanied by minute yellow-greenish flakes (Figs. 5a–d). Additionally, some amygdules are monomineralic, filled only with carbonates.

Microscopic analysis identified the earliest cavity-lining minerals as smectite-group clay minerals (nontronite-saponite) and some chalcedony (Figs. 5a, c). Late magmatic clinopyroxene laths, oriented perpendicular to the cavity walls, are also present in some amygdules (Fig. 5e). The inner infillings are composed of prismatic and bladed/fibrous zeolite crystals (Figs. 5c, d, f). Prismatic zeolites, often altered to an orange-brown dull material,

have low birefringence (~0.01), while bladed/fibrous zeolites, the most common type in SCB amygdules (Figs. 5a, c, f), display orthorhombic symmetry with {110} cleavage visible perpendicular to the crystallographic c-axis (Figs. 5g, i). These zeolites form fan-like aggregates in two main types, distinguished by color and birefringence (Figs. 5a–c, f).

Early-formed fibrous/bladed zeolites are colorless with birefringence up to ~0.02 (Fig. 5c), followed by an epitaxial overgrowth of darker fibrous zeolites with lower birefringence (~0.012 – 0.013), which alter to a brownish dull material (Figs. 5a, c, f). Finally, a second generation of colorless fibrous aggregates forms as an epitaxial overgrowth toward the inner cavity regions (Figs. 5a–c). This pattern resembles the calcic-to-sodic zeolite overgrowth in the natrolite subgroup, as documented by Triana *et al.* (2012) in Isle of Skye basalts, Scotland.

SEM images of SCB amygdules show bladed zeolite crystals (Figs. 5g, i) and petal-like or flake aggregates of nontronite-saponite lining the cavity walls (Fig. 5h). Occasionally, a second generation of clay minerals overgrows the zeolites. Amygdules rich in fibrous zeolites have fewer prismatic crystals, and vice versa.

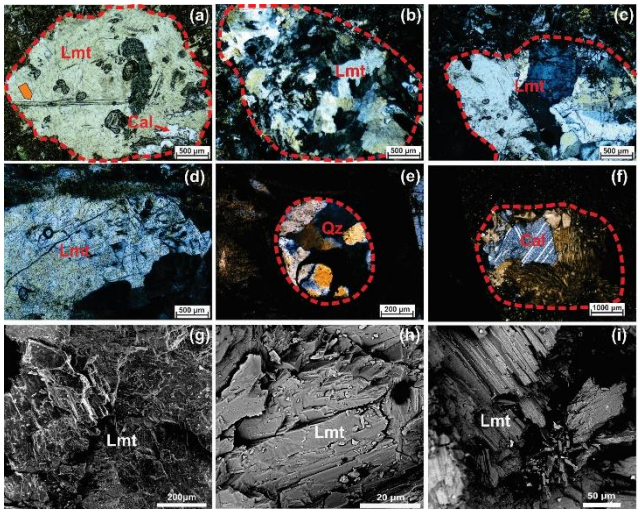

Figure 4. Photomicrographs (a–f) and scanning electron microscopy (SEM) images (g–i) showing textural and morphological aspects of amygdule infillings in the Rio Ceará-Mirim dike swarm. (a–c) Aggregates of subhedral to euhedral crystals of laumontite, minor calcite, and an unidentified fibrous mineral (orange arrow) (samples LM-03.4, LM-03.2, and LM-03); (d) large euhedral laumontite crystals with perfect cleavage in two directions (sample LM-01.2); (e) round-shaped amygdule filled with quartz crystals (sample LM-01.1); (f) calcite associated with unidentified fibrous minerals in an amygdule near fracture zones in the host rock (sample LM-01.2); (g–i) SEM images highlighting the morphology and cleavage planes of laumontite (samples LM-01.2 and LM-03.4). Photomicrograph (a) was obtained using plane-polarized light, while the others were obtained with cross-polarized light. Mineral abbreviations: laumontite (Lmt), calcite (Cal), quartz (Qz).

Figura 4. Fotomicrografias (a–f) e imagens de microscopia eletrónica de varrimento (MEV) (g–i) mostrando aspectos texturais e morfológicos dos preenchimentos das amígdalas no enxame de diques do Rio Ceará-Mirim. (a–c) Agregados de cristais subédricos a euédricos de laumontite, calcite menor e um mineral fibroso não identificado (seta laranja) (amostras LM-03.4, LM-03.2 e LM-03); (d) cristais euédricos de laumontite com clivagem perfeita em duas direcções (amostra LM-01.2); (e) amígdala arredondada preenchida com cristais de quartzo (amostra LM-01.1); (f) calcite associada a minerais fibrosos não identificados numa amígdala próxima de zonas de fraturas na rocha hospedeira (amostra LM-01.2); (g–i) imagens MEV destacando a morfologia e planos de clivagem da laumontite (amostras LM-01.2 e LM-03.4). A fotomicrografia (a) foi obtida com polarizadores paralelos, enquanto as restantes foram obtidas com polarizadores cruzados. Abreviaturas minerais: laumontite (Lmt), calcite (Cal), quartzo (Qz).

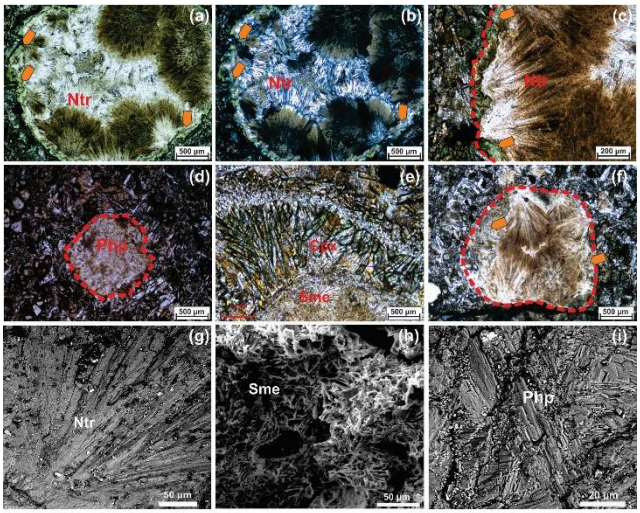

Figure 5. Photomicrographs (a–f) and scanning electron microscopy (SEM) images (g–i) showing textural and morphological aspects of the amygdule infillings in the Serra do Cuó basaltic flow. (a–b) Rounded zoned amygdule with a layer of smectite-group minerals (nontronite-saponite, indicated by orange arrows) lining the cavity wall, followed by two subsequent generations of fibrous/bladed zeolites identified as natrolite-subgroup phases, and late crystals of smectite-group minerals (sample LM-05.2); (c) detail of the amygdule shown in (a); (d) rounded amygdule filled with prismatic phillipsite crystals partially altered to an orange-brown dull material (sample LM-06.2); (e) epitaxial growth of clinopyroxene crystals against the cavity walls, followed by a thin film of unidentified isotropic material (silica?) and fine-grained aggregates of smectite-group minerals (sample LM-05.2); (f) rounded amygdule filled with fibrous Ca-Na zeolites partially altered to a brown dusty material composed of clay minerals; orange arrows indicate layers of smectite-group minerals (nontronite-saponite); (g–i) SEM images detailing the morphology of: (g) fibrous natrolite (sample LM-05.3); (h) petalous and flake aggregates of smectite-group minerals (nontronite-saponite) toward the cavity walls (sample LM-05.3); and (i) bladed crystals of Ca-Na zeolites (sample LM-06.2). Photomicrograph (b) was obtained with cross-polarized light, while the others were obtained using plane-polarized light. Mineral abbreviations: natrolite (Nat), phillipsite (Phl), smectite-group minerals (Sme), clinopyroxene (Cpx).

Figura 5. Fotomicrografias (a–f) e imagens de microscopia eletrónica de varrimento (MEV) (g–i) mostrando aspectos texturais e morfológicos dos preenchimentos das amígdalas no derrame basáltico Serra do Cuó. (a–b) Amígdala arredondada zonada com uma camada de minerais do grupo das esmectites (nontronite-saponite, indicada por setas laranjas) revestindo a parede da cavidade, seguida por duas gerações de zeolitas fibrosos/laminares identificados como fases do subgrupo natrolite, e cristais tardios de minerais do grupo das esmectites (amostra LM-05.2); (c) detalhe da amígdala mostrada em (a); (d) amígdala arredondada preenchida com cristais prismáticos de phillipsite, parcialmente alterados para um material baço castanho-alaranjado (amostra LM-06.2); (e) crescimento epitaxial de cristais de clinopiroxena contra as paredes da cavidade, seguido por uma película fina de material isotrópico não identificado (sílica?) e agregados finos de minerais do grupo das esmectites (amostra LM-05.2); (f) amígdala arredondada preenchida com zeolitas fibrosos de Ca-Na, parcialmente alterados para um material poeirento castanho composto por minerais argilosos; as setas laranjas indicam camadas de minerais do grupo das esmectites (nontronite-saponite); (g–i) imagens MEV detalhando a morfologia de: (g) natrolite fibrosa (amostra LM-05.3); (h) agregados petalóides e lamelares de minerais do grupo das esmectites (nontronite-saponite) nas paredes da cavidade (amostra LM-05.3); e (i) cristais laminares de zeolitas de Ca-Na (amostra LM-06.2). A fotomicrografia (b) foi obtida com polarizadores cruzados, enquanto as restantes foram obtidas com polarizadores paralelos. Abreviaturas minerais: natrolite (Nat), phillipsite (Phl), minerais do grupo das esmectites (Sme), clinopiroxena (Cpx).

4.2 Mineralogical identification

4.2.1 Rio Ceará-Mirim dike swarm

XRD analysis of CMD cavity infillings (Figs. 6a–c) shows laumontite as the dominant zeolite, with peaks characteristic of laumontite at 2θ = 9.36°, 12.95°, 21.41°, and 25.43° (d-spacings of 9.445, 6.835, 4.150, and 3.503 Å) (Fridriksson *et al*., 2003; Lee *et al*., 2004), consistent with microscopic observations. Secondary

minerals include quartz and possible trace amounts of chabazite, though its presence lacks sufficient textural and chemical evidence for confirmation. Peaks for plagioclase and diopside suggest possible contamination from the host rock primary mineralogy during cavity scraping.

Mineral chemical analysis (Tab. 2; Fig. 7) confirmed laumontite as the primary mineral in CMD amygdules, showing relatively homogeneous compositions with slight variations in CaO content (9.82 – 12.4 wt.%). The composition fits within the laumontite field on the ternary classification diagram $10(SiO_2 / Al_2O_3) – (CaO + MgO) – (Na_2O + K_2O)$ (Fig. 7a; Bastias *et al.* (2016). The calculated structural formula is:

$[Ca_{3.34-4.26}Na_{0.23}K_{0.08-0.23}Fe_{0.08}]_{\Sigma=3.34-4.41}[Al_{7.6-7.96}Si_{15.96-16.4}O_{48}].18H_2O,$

and the Si/(Si + Al) ratio values range from 0.67 to 0.68.

The TGA curve of sample LM 01.2 (Fig. 8a) revealed three dehydration peaks at 109.7 °C (1.3% H_2O loss), 234.1 °C (5% H_2O loss), and 380 °C (5.9% H_2O loss), indicating laumontite's stability over a range of temperatures. These peaks align with the typical stepwise dehydration of laumontite at ~100 °C, ~240 °C, and ~400 °C, and its partial transformation into leonhardite (Gottardi and Galli, 1985; Deer *et al*., 2013). This confirms laumontite as the primary zeolite in the CMD amygdules.

4.2.2 Serra do Cuó basaltic flow

XRD analysis of sample LM 05.3 (Fig. 6d) identifies natrolite as the dominant zeolitic phase, with minor amounts of phillipsite, smectite (nontronite-saponite), and quartz/chalcedony. Key natrolite peaks are observed at $2\theta = 6.85°$, 13.56°, 14.98°, 20.35°, 28.24°, 28.89°, and 31.24° (d-spacings of 12.904, 6.528, 5.914, 4.364, 3.160, 3.091, and 2.863 Å) (Krogh Andersen *et al*., 1990; Stuckenschmidt *et al*., 1996; Hassan and Al-Rashed, 2020). Phillipsite peaks are weaker and partially overlap with natrolite peaks at $2\theta = 18.02°$, 28.02°, and 28.49° (d-spacings of 4.923, 3.184, and 3.133 Å; Gatta *et al*., 2009). A broad reflection near $2\theta \approx 6.3°$ (~14 Å) and peaks at $2\theta = 9.17°$ and 21.34° (d-spacings of 9.644 and 4.164 Å) correspond to smectite-group minerals.

These findings align with the microscopic textural characterization and optical properties, which show that most SCB cavities are lined with nontronite-saponite and filled with prismatic and fibrous/bladed zeolite crystals (Figs. 5a-c). The fibrous/bladed crystals are identified as natrolite (Fig. 5g), while the prismatic crystals correspond to phillipsite (Fig. 5i).

Table 2. Representative semi-quantitative chemical compositions of zeolites in amygdules from the Rio Ceará-Mirim dike swarm and the Serra do Cuó basaltic flow. *H_2O contents are based on ideal zeolite structural formulae. < dl: values below detection limits. E% = [(Al + Fe^{3+}) - Altheor / Altheor] * 100, where Altheor = (Na + K) + 2*(Ca + Mg + Ba + Sr) (Passaglia, 1970).

Tabela 2. Composições químicas representativas semi-quantitativas de zeolitas em amígdalas do enxame de diques Rio Ceará-Mirim e do derrame basáltico Serra do Cuó. Os teores de H_2O são baseados nas fórmulas estruturais ideais de zeolitas. <dl: valores abaixo dos limites de deteção. E% = [(Al + Fe^{3+}) – Altheor / Altheor] * 100, onde Altheor = (Na + K) + 2(Ca + Mg + Ba + Sr) (Passaglia, 1970).

Rock	**Rio Ceará-Mirim dike swarm**						**Serra do Cuó basaltic flow**				
Sample	LM 01.2	LM 03.2	LM 03.4		LM 04.2		LM 05.3		LM 06.2		
Crystal	c.1	c.2	c.3	c.4	c.5		c.1		c.2	c.3	c.4
Analysis	s.9	s.66	s.25	s.30	s.42	s.44	s.13	s.12	s.57	s.60	s.62
Zeolites	laumontite						natrolite-subgroup			phillipsite-subgroup	
SiO_2(wt.%)	50.78	50.72	49.80	50.50	50.56	51.64	48.90	48.01	48.71	44.45	42.64
Al_2O_3	21.04	21.22	20.53	21.02	20.15	20.69	25.14	25.65	26.79	25.28	26.11
Fe_2O_3	0.32	<dl	0.32	<dl	0.32	<dl	<dl	<dl	<dl	0.32	<dl
MgO	0.00	<dl	0.17	<dl	<dl	<dl	0.78	0.78	0.36	<dl	<dl
CaO	10.90	10.66	12.40	11.56	11.97	9.82	1.15	2.00	1.75	4.33	6.79
Na_2O	<dl	<dl	<dl	<dl	<dl	0.37	14.54	14.04	12.83	9.20	8.00
K_2O	<dl	0,56	<dl	<dl	0,19	0,56	<dl	<dl	<dl	<dl	<dl
Total	83.04	83.16	83.21	83.08	83.19	83.09	90.52	90.48	90.44	83.58	83.55
H_2O*	16.90	16.90	16.90	16.90	16.90	16.90	9.50	9.50	9.50	16.50	16.50
	cationic proportions based on 48 oxygens						cationic proportions based on 80 oxygens				
Si (cpfu)	16.164	16.152	15.960	16.101	16.175	16.404	24.643	24.263	24.407	24.103	23.286
Al	7.892	7.962	7.753	7.900	7.596	7.748	14.934	15.282	15.829	16.161	16.12
Fe^{3+}	0.077	-	0.077	-	0.077	-	-	-	-	0.132	-
Mg	-	-	0,079	-	-	-	0.586	0.588	0.269	-	-
Ca	3.719	3.638	4.257	3.948	4.101	3.344	0.622	1.083	0.938	2.519	3.972
Na	-	-	-	-	-	0.228	14.209	13.759	12.469	9.671	8.475
K	-	0.228	-	-	0.078	0.227					
Σcations	27.852	27.980	28.125	27.949	28.027	27.950	54.994	54.975	53.913	52.586	52.545
E%	7.1	6.1	-9.7	0.1	-7.3	8.5	-10.2	-10.6	6.4	10.8	2.4
Si/(Si+Al)	0.67	0.67	0.67	0.67	0.68	0.68	0.62	0.61	0.61	0.60	0.58

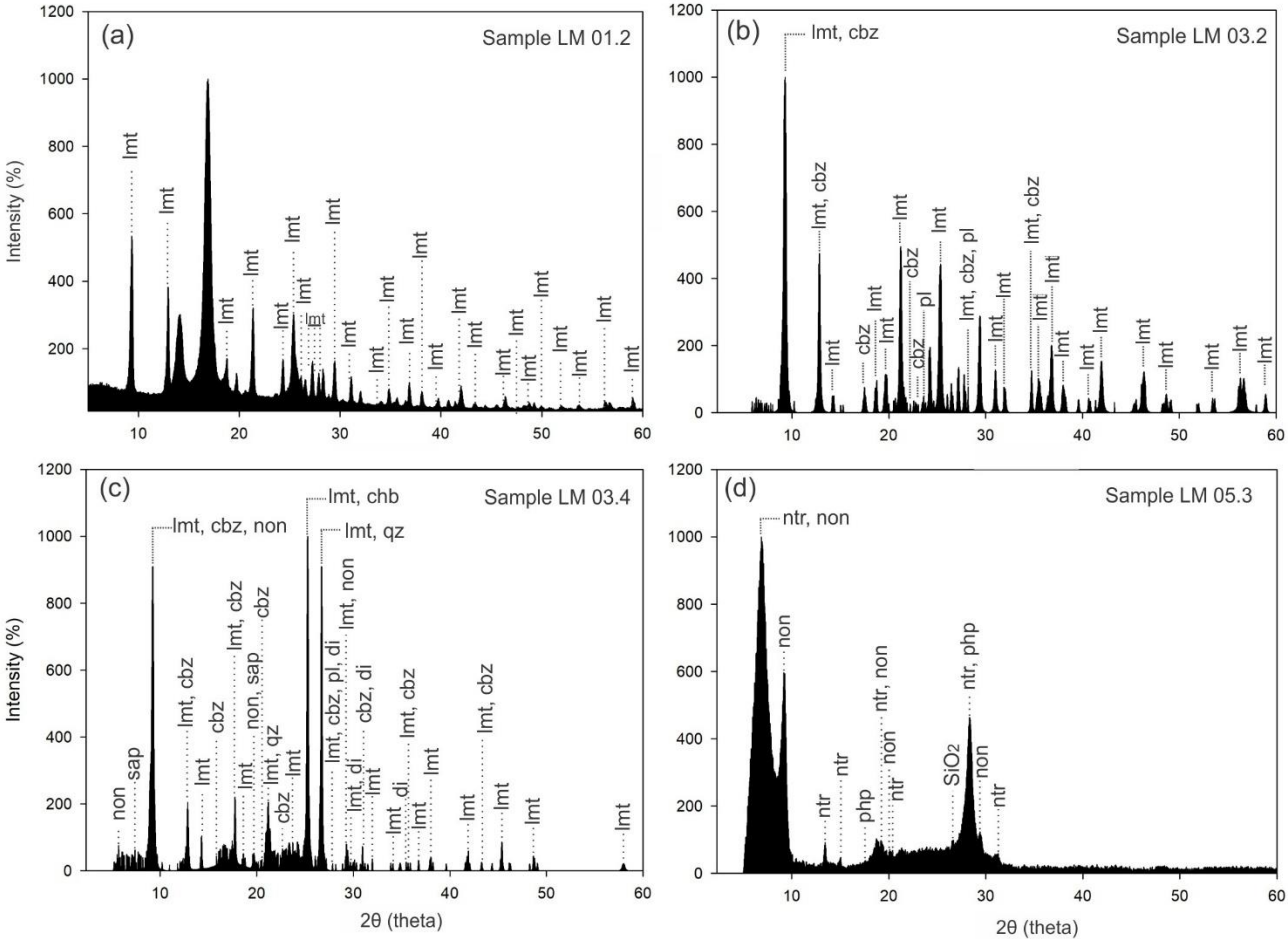

Figure 6. X-ray diffraction (XRD) patterns showing the occurrence of zeolites and other minor phases in the studied amygdules from the Rio Ceará-Mirim dike swarm (a-c), and from the Serra do Cuó basaltic flow (d). The identified phases include laumontite (lmt), chabazite (cbz), natrolite (ntr), phillipsite (phl), nontronite (non), saponite (sap), plagioclase (pl), and diopside (di).

Figura 6. Padrões de difração de raios X (DRX) mostrando a ocorrência de zeolitas e outras fases menores nas amígdalas estudadas do enxame de diques Rio Ceará-Mirim (a-c) e do derrame basáltico Serra do Cuó (d). As fases identificadas incluem laumontite (lmt), chabazite (cbz), natrolite (ntr), phillipsite (phl), nontronite (non), saponite (sap), plagioclase (pl) e diopsídio (di).

Mineral chemical analyses were performed on amygdules from samples LM 05.3 and LM 06.2 (Tab. 2). Bladed (sample LM 05.3) and prismatic crystals (sample LM 06.2) were identified in the SEM images (Figs. 5g, i). Analyses with $E < 10\%$ for LM 05.3 showed compositions close to natrolite (Fig. 7), with a calculated structural formula (considering the ideal stoichiometric water content of 9.5 wt.% for this zeolite; cf. Gottardi and Galli, 1985; Coombs *et al.*, 1997) of:

$$[Na_{12.47\text{-}14.21}Ca_{0.62\text{-}1.08}Mg_{0.27\text{-}0.59}]_{\Sigma=13.68\text{-}15.43}Al_{14.93\text{-}15.83}Si_{24.27\text{-}24.64}O_{80}.16H_2O,$$

and Si / (Si + Al) ratio between 0.61–0.62.

However, Ca levels are slightly higher than typical for natrolite, which usually has low Ca content (< 1.0 cpfu) (Birch, 1989; Kónya and Szakáll, 2011; Özen and Göncüoğlu, 2015; Mattioli *et al*., 2016). This suggests compositions potentially intermediate between natrolite and Ca-Na-bearing gonnardite or mesolite (Figs. 7a and 9), though further studies are required to confirm this. Additionally, optical microscope images reveal distinct generations of fibrous/bladed crystals exhibiting overgrowth relationships akin to those between calcic and sodic zeolites in the natrolite subgroup (Figs. 5c, f), as described by Triana *et al*. (2012).

The TGA curve for sample LM 05.3 (Fig. 8b) shows dehydration peaks at 90.5 °C (2.3% H_2O loss), 360 °C (6% H_2O loss), and 866 °C (5% H_2O loss). The first peak aligns with smectite dehydration, typical between 100 and 200 °C (Földvári, 2011), while the second peak corresponds to natrolite dehydration, generally between 340 – 400 °C. The third peak, at 866 °C, likely represents dehydroxylation or structural breakdown of smectite with subsequent new phase crystallization (Földvári, 2011). These results indicate that natrolite is the primary zeolite in SCB amygdules, with minor amounts of smectite-group minerals.

In sample LM 06.02, zeolites showed higher Al (16.16 – 16.81 cpfu) and Ca (2.52 – 3.97 cpfu) contents, with lower Na (8.47 – 9.67 cpfu). These compositions plot near the phillipsite field on the Si/Al versus (K + Na) / (K + Na + Ca) discrimination diagram (Chipera and Apps, 2001; Fig. 7b). Assuming an ideal stoichiometric water content of 16.5 wt.% for this zeolite subgroup (Gottardi and Galli, 1985; Coombs *et al*., 1997), the calculated structural formula is:

$[Na_{8.47-9.67}Ca_{2.52-3.97}Ca_{2.52-3.97}Fe_{0.13}]_{\Sigma=12.3-12.4}Al_{16.16-16.81}Si_{23.29-24.1}O_{80}.30H_2O$,

with Si / (Si + Al) ratios ranging from 0.58 to 0.60.

Mafic phyllosilicates (clay minerals) also play a significant role in filling SCB amygdules. Optical and SEM images (Fig. 5) show these minerals primarily as early aggregates with petal-like crystal growth along cavity walls, later forming overgrowths on the zeolites. XRD patterns (Fig. 6d) confirm that these mafic

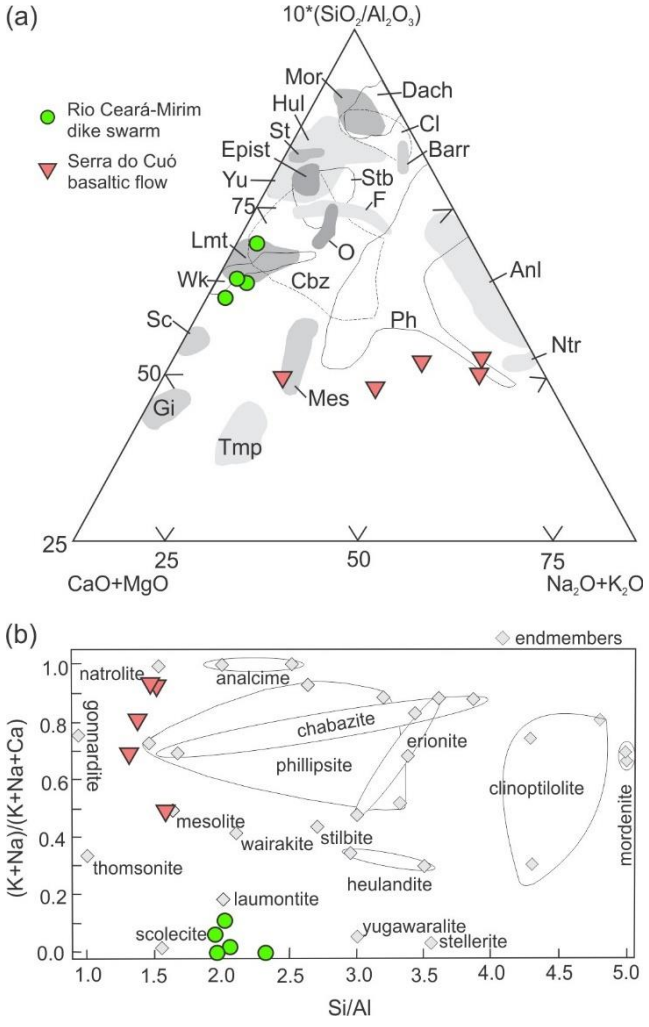

Figure 8. Chemical compositions of the analyzed zeolites. (a) Projection on the chemical system $10(SiO_2 / Al_2O_3) – (CaO + MgO) – (Na_2O + K_2O)$ (wt%) based on Bastias *et al.* (2016); (b) projection on the discriminating cationic diagram Si / Al vs. (K + Na) / (K + Na + Ca) based on Chipera and Apps (2001). Abbreviations in (a): analcime (Anl), barrerite (Bar), clinoptilolite (Cpt), dachiardite (Dac), epistilbite (Epi), faujasite (Fau), gismondine (Gis), heulandite (Heu), laumontite (Lmt), mesolite (Mes), mordenite (Mor), natrolite (Nat), offretite (Off), scolecite (Sco), stellerite (Ste), stilbite (Stb), thomsonite (Tho), wairakite (Wai), yugawaralite (Yug).

Figura 8. Composições químicas dos zeolitas analisados. (a) Projecção no sistema químico $10(SiO_2 / Al_2O_3) – (CaO + MgO) – (Na_2O + K_2O)$ (% em massa) baseado em Bastias *et al.* (2016); (b) projecção no diagrama catiónico discriminante Si/Al versus (K + Na)/(K + Na + Ca) baseado em Chipera e Apps (2001). Abreviaturas em (a): analcima (Anl), barrerita (Bar), clinoptilolite (Cpt), dachiardite (Dac), epistilbite (Epi), faujasite (Fau), gismondina (Gis), heulandite (Heu), laumontite (Lmt), mesolite (Mes), mordenite (Mor), natrolite (Nat), offretite (Off), escolecite (Sco), estellerite (Ste), estilbite (Stb), thomsonite (Tho), wairakite (Wai), yugawaralite (Yug).

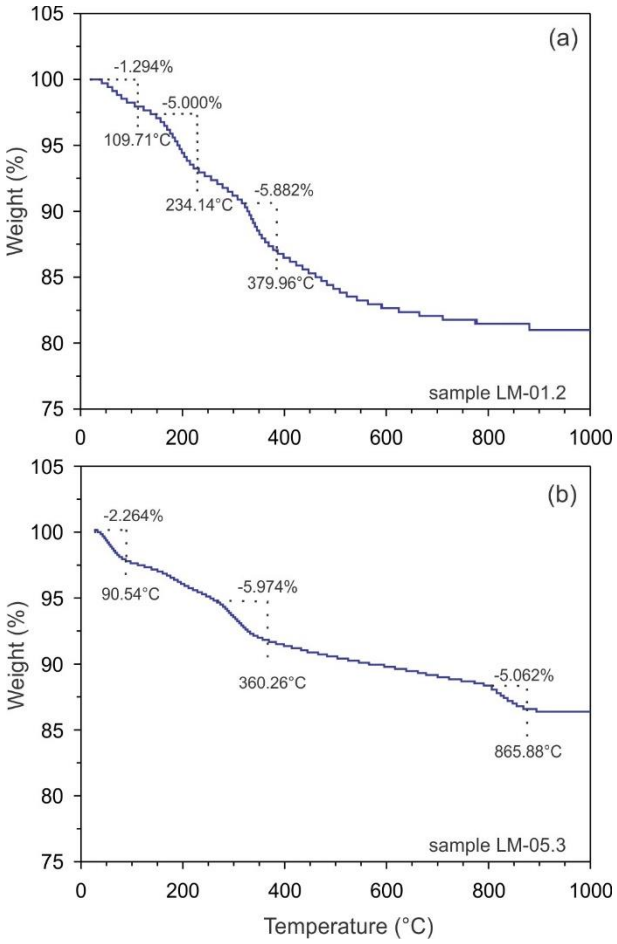

Figure 7. Thermogravimetric (TGA) curves for minerals filling cavities in the Rio Ceará-Mirim and Serra do Cuó basaltic rocks. (a) Laumontite in amygdules of the Rio Ceará-Mirim dike swarm (sample LM-01.2); (b) natrolite and nontronite-saponite in amygdules of the Serra do Cuó basaltic flow (sample LM-05.3).

Figura 7. Curvas termogravimétricas (TGA) para minerais preenchendo cavidades nas rochas basálticas Rio Ceará-Mirim e Serra do Cuó. (a) Laumontite em amígdalas do enxame de diques do Rio Ceará-Mirim (amostra LM-01.2); (b) natrolite e nontronite-saponite em amígdalas do derrame basáltico da Serra do Cuó (amostra LM-05.3).

phyllosilicates closely align with the nontronite-saponite series (Dainyak *et al*., 2006), with an average composition of:

$[Ca_{0.68}Na_{0.5}]_{\Sigma=1.18}[Mg_{4.75}Fe_{0.34}Al_{0.49}]_{\Sigma=5.58}[Si_{6.7}Al_{1.23}]_{\Sigma=7.93}O_{20}(OH)_4$.

5. Discussion

The alteration of volcanic and subvolcanic rocks by hot hydrothermal fluids or meteoric water is a well-documented process, seen in regions such as the North Atlantic Igneous Province and Deccan Traps (India). These alteration processes dissolve primary magmatic phases, enabling the precipitation of secondary minerals. This process depends on the rock mineralogy and composition, fluid chemistry, and temperature-pressure conditions (*e.g.*, Walker, 1960; Kristmannsdóttir and Tomasson, 1978; Robert, 2001).

Primary minerals in basaltic rocks, including olivine, pyroxenes, Ca-plagioclase, and Fe-Ti oxides, as well as interstitial glass, become metastable, leading to dissolution and hydrolysis

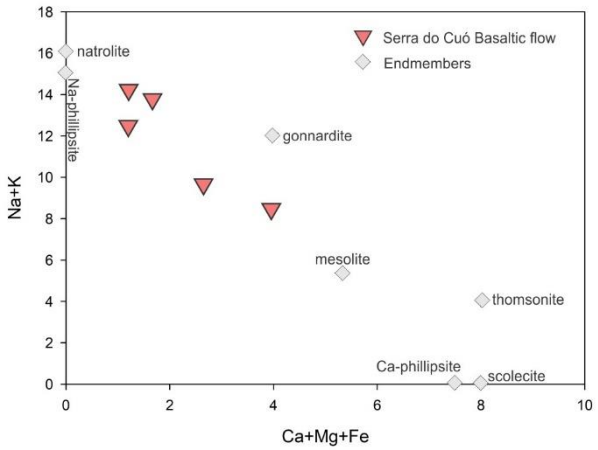

Figure 9. Binary cationic plot of Ca + Mg + Fe versus Na + K for the Ca – Na zeolites in amygdules of the Serra do Cuó basalts. Ideal zeolite end-member compositions (Coombs *et al.*, 1997; Deer *et al.*, 2013) are shown as solid grey diamonds.

Figura 9. Diagrama catiónico binário de Ca + Mg + Fe versus Na + K para os zeolitas Ca – Na nas amígdalas dos basaltos da Serra do Cuó. As composições ideais dos membros finais dos zeolitas (Coombs *et al.*, 1997; Deer *et al.*, 2013) estão indicadas como diamantes cinzas.

that release chemical components (*e.g.*, Mg, Fe, Ca, Si, and Al) into fluids. Under low-temperature conditions, these components then precipitate as secondary minerals, such as clays and zeolites (Honnorez, 1978; Eggleton *et al.*, 1987; Chipera and Apps, 2001; Kónya and Szakáll, 2011; Abdioglu, 2012; Bastias *et al.*, 2016; Mattioli *et al.*, 2016; Ottens *et al.*, 2019).

The presence of secondary, water-rich minerals within amygdules of the CMD and SCB basalts and microgabbros suggests that hot fluids circulated through these rocks, decomposing primary minerals. The CMD and SCB exhibit distinct secondary mineral assemblages, indicating that host rock composition influences alteration pathways: CMD is subalkaline and Fe-rich, while SCB is alkaline and Mg-rich (Fig. 2). Furthermore, the subvolcanic crystallization environment of CMD rocks contrasts with the extrusive nature of SCB flows, suggesting variations in the processes and fluids involved.

5.1 Alteration processes and secondary mineral formation in the Ceará-Mirim dike swarm

In the CMD rocks, the primary magmatic phases and basaltic glass were replaced by white mica, smectites, Fe-oxyhydroxides, and calcite (Fig. 10a). The vesicles are mainly filled with euhedral laumontite (a Ca-rich zeolite), although calcite and quartz are also present. This indicates the percolation of aqueous fluids through the rock system, which was enriched primarily in Si, Al, and Ca, along with minor amounts of Mg and Fe, derived from the destabilization of primary mafic silicates, glass, and Ca-rich plagioclase (Fig. 10a). Based on this secondary mineral assemblage, it is suggested that hydrothermal alteration in the CMD occurred in two stages at different temperatures, referred to as Stages I and II (Figs. 11a and 12).

The occurrence of accessory biotite and amphibole in some samples indicates crystallization from hydrous melts (containing approximately 4-7 wt% H_2O; Sisson and Grove, 1993; Moore and Carmichael, 1998; Pichavant and Macdonald, 2007) during the late stages of CMD emplacement, though not necessarily implying water saturation or the exsolution of free magmatic water. Stage I is characterized by the pervasive destabilization of reactive glass, Ca-plagioclase, and mafic minerals, most likely resulting from the interaction of rocks with heated meteoric waters drawn in by the convective cooling of the dikes at shallow crustal levels (Bindeman *et al.*, 2020; Fig. 12). While a contribution from magmatic fluids cannot be entirely ruled out, the observed mineral assemblage is consistent with meteoric fluid-dominated alteration.

During Stage I, the formation of white mica as an alteration product of primary phases indicates temperatures likely below 300 °C, as the absence of higher-grade minerals typical of greenschist or amphibolite facies (such as actinolite, albite, epidote, or chlorite) constrains the upper temperature limit of alteration (Galán and Ferrell, 2013; Verati and Jourdan, 2014). Experiments

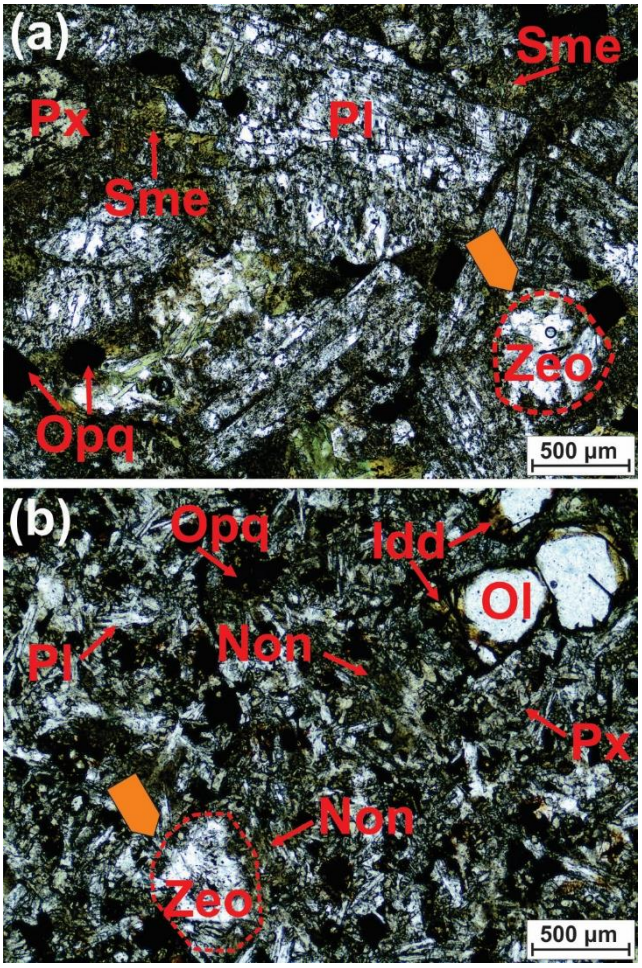

Figure 10. Photomicrographs of host-rock mineralogy highlighting the superimposed hydrothermal alteration. (a) Detail of a Rio Ceará-Mirim microgabbro showing primary clinopyroxene, plagioclase and oxides replaced mainly by greenish smectite-group minerals; (b) detail of a Serra do Cuó basalt showing the primary mineralogy of olivine, plagioclase, clinopyroxene and oxides replaced by "iddingsite" and smectite-group minerals. Orange arrows point to zeolite-filled amygdules. Mineral abbreviations: pyroxene (Px), plagioclase (Pl), olivine (Ol), opaque minerals (Opq), smectite-group minerals (Sme), zeolites (Zeo), "iddingsite" (Idd). Photomicrographs obtained under plane polarized light.

Figura 10. Fotomicrografias da mineralogia da rocha hospedeira destacando a alteração hidrotermal sobreposta. (a) Detalhe de um microgabro Rio Ceará-Mirim mostrando clinopiroxena, plagioclase e óxidos primários substituídos principalmente por minerais esverdeados do grupo das esmectites; (b) detalhe de um basalto Serra do Cuó mostrando a mineralogia primária de olivina, plagioclase, clinopiroxena e óxidos substituídos por "iddingsite" e minerais do grupo das esmectites. Setas laranjas indicam amígdalas preenchidas com zeolitas. Abreviaturas minerais: piroxena (Px), plagioclase (Pl), olivina (Ol), minerais opacos (Opq), minerais do grupo das esmectites (Sme), zeolitas (Zeo), "iddingsite" (Idd). Fotomicrografias obtidas com polarizadores cruzados.

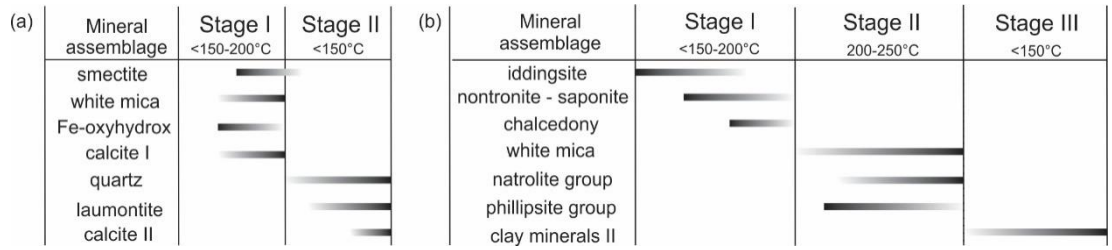

Figure 11. Stages of secondary mineral formation in cavities of (a) Rio Ceará-Mirim and (b) Serra do Cuó basaltic rocks.

Figura 11. Etapas de formação de minerais secundários em cavidades das rochas basálticas (a) do Rio Ceará-Mirim e (b) da Serra do Cuó.

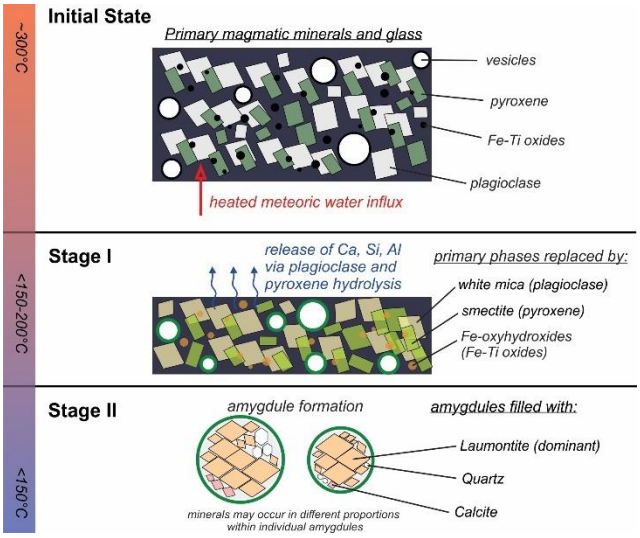

Figure 12. Sketch (not to scale) illustrating the sequence of secondary mineral neoformation within amygdules in the basalts of the Rio Ceará-Mirim dyke swarm.

Figura 12. Esquema (fora de escala) ilustrando a sequência de neoformação de minerais secundários nas amígdalas dos basaltos do Enxame de Diques Rio Ceará-Mirim.

by Larsen *et al.* (1991; see also Baldermann *et al.*, 2014) demonstrated that smectite-group minerals form by the alteration of basaltic rocks at 150 – 200 °C. However, Alt *et al.* (2010) documented that basaltic lavas at the East Pacific Rise are altered to smectite-group minerals at temperatures < 150 °C to near-ambient conditions, confirming that these phases can form at substantially lower temperatures. This aligns with our interpretation of progressive cooling during alteration and supports the possibility of mineral formation across a broader temperature range. Therefore, Stage I likely represents a low to moderate-temperature (< 150 – 200 °C) hydrothermal event dominated by heated meteoric waters that altered primary minerals and released chemical components during water-rock interaction (Fig. 11a). Notably, mafic phyllosilicates were absent as cavity linings in CMD rocks.

Stage II is characterized by the formation of laumontite, quartz, and some calcite within cavities at temperatures < 150 °C (Figs. 11a and 12). The destabilization of primary minerals could be enhanced by the influx of relatively cool meteoric waters, releasing more Ca, Si, and Al—for instance, through the plagioclase hydrolysis reaction, as follows:

$$CaAl_2Si_2O_8 + H^+ \leftrightarrow HAlSi_3O_8 + Ca^{2+} \quad \text{(Eq. 1)}$$

The released elements were used for laumontite, quartz, and calcite precipitation inside cavities (Fig. 12). Moreover, the formation of calcite also suggests the presence of dissolved CO_3^{2-} in the fluids. Further calcium supply could be derived from the alteration of Ca-rich basaltic glass in the CMD (cf. Archanjo *et al.*, 2002).

According to Liou *et al.* (1991; see also Kristmannsdóttir, 1979), laumontite typically forms at temperatures > 150 °C, reaching ~260 °C. However, when it occurs in paragenesis with quartz, as observed in the CMD (Figs. 4e, 6c), laumontite precipitation temperatures can decrease to as low as 125 °C (Fridriksson *et al.*, 2003; Figs. 11a and 12).

5.2 Alteration processes and secondary mineral formation in the Serra do Cuó basaltic flow

The SCB secondary mineralogy reveals a complex, chemically distinct, multistage hydrothermal alteration sequence. Moreover, augite laths ('miarolitic minerals' *sensu* Kónya and Szakáll, 2011) occasionally crystallized along cavity walls (Fig. 5e) during a late magmatic stage at temperatures up to 600 °C (Kónya and Szakáll, 2011), distinct from subsequent secondary alteration processes.

The assemblage of mafic phyllosilicates and zeolites observed in SCB amygdules is characteristic of zeolite facies metamorphism (anchimetamorphism) in basalts, similar to that seen in the Paraná Volcanic Province, Brazil (Duarte *et al.*, 2009; Hartmann *et al.*, 2012), the North Atlantic Tertiary Igneous Province (Walker, 1960; Neuhoff, 1999), the Deccan Traps, India (Ottens *et al.*, 2019), and the Kahrizak volcanic field, Iran (Kusehlar *et al.*, 2010; Kousehlar *et al.*, 2012).

As noted by Ottens *et al.* (2019), the cooling of recently erupted flows is commonly followed by intense rock–water (mainly meteoric) interactions, leading to the initial alteration of more reactive glass and mafic minerals. The alteration of basaltic glass results in cation leaching in the order Na > Mg > K > Ca > Al > Fe (Eggleton *et al.*, 1987; Jeong and Sohn, 2011). The hydrolysis reaction of olivine and clinopyroxene can be written as:

$$(Fe,Mg)_2SiO_4 + Ca(Mg,Fe)Si_2O_6 + 4H_2O + 2H^+ \leftrightarrow (Mg^{2+},Fe^{2+}) + Ca^{2+} + (Mg^{2+},Fe^{2+}) + 2SiO_2 + Si(OH)_{4aq} + 6(OH)^- \quad \text{(Eq. 2)}$$

This reaction provides the main components for forming smectite-group minerals (nontronite/saponite) that line the vesicle walls during an early low-temperature alteration stage (Stage I; Figs. 11b and 13). These clay minerals can form over a broad temperature range, from near-ambient conditions to below 150 °C and up to 200 °C (Baker and Haggerty, 1967; Seyfried and Bischoff, 1979; Larsen *et al.*, 1991; Alt *et al.*, 2010; Fig 11a). Additionally, olivine is

replaced by '*iddingsite*' (Fig. 10b), indicating alteration under oxidizing conditions at temperatures < 140 °C (Baker and Haggerty, 1967). As smectite precipitates, Mg and Fe concentrations decrease relative to Ca, along with a reduction in Si/Al ratios. Compared to glass and olivine, plagioclase is more stable under low-temperature metamorphic conditions and undergoes hydrolysis later, releasing Ca and Na into the solution, as shown in reactions such as those by Kousehlar *et al*. (2012):

$$Ca_3Na_2Al_8Si_{12}O_{40} + H_2O \leftrightarrow 3Ca^{2+} + 2Na^{+} + 8AlO_2^{-} + 12SiO_2 + H_2O \quad \text{(Eq. 3)}$$

This change in fluid composition initiated a second hydrothermal stage (Stage II; Figs. 11b and 13), marked by the formation of euhedral fibrous and bladed Na-Ca zeolites, primarily from the phillipsite and natrolite subgroups (Figs. 5 and 13), directly over Stage I minerals, alongside plagioclase alteration to white mica. While clay minerals typically form around pH ~7, most zeolites form at pH > 9 (Nemecz, 1981; Stefánsson and Gislason, 2001; Kousehlar *et al*., 2012), suggesting the fluid evolved to more alkaline conditions, consistent with the host rock composition (Fig. 2a). In contrast, acidic fluids would favor quartz precipitation (Kousehlar *et al*., 2012), a mineral rarely observed in SCB secondary paragenesis.

The shift from Stage I to Stage II (Fig. 13), indicating a change in aqueous solution chemistry (Kónya and Szakáll, 2011; Mattioli *et al*., 2016), may also reflect a slight temperature increase (Kousehlar *et al*., 2012; Ottens *et al*., 2019), potentially due to the burial of volcanic rock or late magmatic events in the region (cf. Neuhoff, 1999; Kousehlar *et al*., 2012). Pe-Piper and Miller (2003) suggest that Ca-bearing zeolites more commonly form from higher-temperature solutions than Na-zeolites, though the reverse has been observed in many amygdaloidal basalts globally (*e.g.*, Kónya and Szakáll, 2011; Triana *et al*., 2012).

Experimental data on zeolite formation from basaltic glass indicate that phillipsite is stable up to 150 – 200 °C (Kristmannsdóttir and Tomasson, 1978; Barth-Wirsching and Hoeller, 1989), while natrolite remains stable in Si-deficient systems at temperatures up to 250 °C (Senderov, 1988). Thus, Stage II alteration in SCB likely occurred at moderately elevated temperatures of around 200 – 250 °C. Finally, a distinct Stage III, identifiable by a second-generation low-temperature clay mineral replacing zeolites in some amygdules, likely reflects the influx of cooler meteoric water (Figs. 11b and 13).

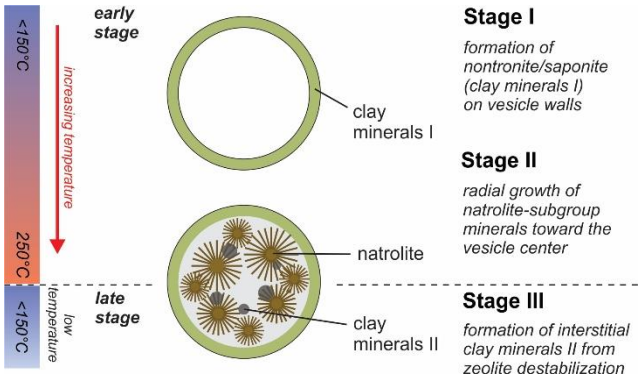

Figure 13. Sketch (not to scale) illustrating the sequence of secondary mineral neoformation within amygdules in the Serra do Cuó basalts.

Figura 13. Esquema (fora de escala) ilustrando a sequência de neoformação de minerais secundários nas amígdalas dos basaltos Serra do Cuó.

6. Conclusions

The amygdule-filling secondary mineral assemblages in Mesozoic subalkaline and alkaline tholeiitic basalts and microgabbros from the Rio Ceará-Mirim dike swarm (CMD) and the Serra do Cuó basaltic flow (SCB) in the northern part of the Borborema Province, Northeastern Brazil, were characterized through petrography, X-ray diffraction, thermogravimetry, and in situ chemical analysis.

In the Fe-rich, subalkaline CMD rocks, amygdules range from millimeters to centimeters in irregular, elongated, or ellipsoidal shapes. These cavities are primarily monomineralic, filled mainly with euhedral tabular or prismatic zeolites, quartz, and minor calcite. Diffraction, thermogravimetric, and chemical analyses confirmed laumontite as the primary zeolite, which precipitated at ~125 °C during a low-temperature hydrothermal stage (Stage II). This followed an earlier alteration stage (Stage I), in which primary minerals were replaced by phyllosilicates at low to moderate temperatures (< 150 – 250 °C).

In contrast, the Mg-rich, alkaline SCB basalts contain millimeter-sized, rounded amygdules, typically polymineralic and indicative of a complex, multistage hydrothermal process. Early, authigenic phases (Stage I) include mafic phyllosilicates (mainly from the nontronite-saponite series), which replaced primary minerals and lined cavity walls. These clay minerals formed across a wide temperature range, from near-ambient conditions to ~200 ºC. A subsequent hydrothermal stage (Stage II) led to the precipitation of prismatic and fibrous/bladed zeolite aggregates. X-ray diffraction and chemical data identified these as Ca-Na zeolites from the phillipsite and natrolite subgroups, reflecting fluid composition changes and slightly higher formation temperatures (up to 250 °C). In a later stage (Stage III), zeolites were partially replaced by clay minerals, marking a lower-temperature phase.

Mafic phyllosilicates and zeolites in CMD and SCB rocks result from the dissolution and hydrolysis of primary minerals, driven by heated meteoric fluids. The similar temperature ranges for secondary mineral formation in both rocks suggest that fluid composition, rather than temperature, is the primary factor influencing mineral variation in amygdules. Differences in fluid composition align with the distinct chemical and mineralogical properties of the host rocks: the Mg-rich, alkaline SCB rocks contrast with the laumontite-filled cavities in the Fe-rich, subalkaline CMD rocks, underscoring the importance of host-rock composition in determining amygdule mineralogy.

Acknowledgments

The authors thank the Programa de Pós-Graduação em Geodinâmica e Geofísica at the Universidade Federal do Rio Grande do Norte (PPGG-UFRN) for both logistical and financial support. We also express our gratitude to the laboratory teams at LACAMM (IFRN), LDN (UFPE), DRX-DFTE, LABPEMOL, and LaPFiMC (UFRN). Special thanks to Drs. Carla J. S. Barreto (UFPE) and Rafael R. Fillippi (IFRN) for their assistance with chemical data acquisition. This study was partially funded by the Coordenação de Aperfeiçoamento de Pessoal de Nível Superior, Brasil (CAPES), Finance Code 001. We are grateful to Dr. Colombo C. G. Tassinari (Editor) and Dr. Ana de Jesus for their constructive reviews, which significantly improved the quality of this manuscript. We also acknowledge the editorial handling by Ms. Susana Machado.

References

Abdioglu, E., 2012. Mineralogy and chemistry of zeolites and associated minerals in tertiary alkaline volcanics from the Eastern Pontides, NE Turkey. *Neues Jahrbuch für Mineralogie - Abhandlungen* **189**(1): 35–47. https://doi.org/10.1127/0077-7757/2011/0208.

Almeida, F. F. M., Hasui, Y., Brito Neves, B. B., Fuck, R. A., 1981. Brazilian structural provinces: An introduction. *Earth-Science Reviews* **17**(1–2): 1–29. https://doi.org/10.1016/0012-8252(81)90003-9.

Alt, J. C., Laverne, C., Coggon, R. M., Teagle, D. A. H., Banerjee, N. R., Morgan, S., Smith-Duque, C. E., Harris, M., Galli, L., 2010. Subsurface structure of a submarine hydrothermal system in ocean crust formed at the East Pacific Rise, ODP/IODP Site 1256. *Geochemistry, Geophysics, Geosystems*, **11**: Q10010. https://doi.org/10.1029/2010GC003144.

Angelim, L. D. A., Nesi, J. D., Torres, H. H. F., Medeiros, V. C., Santos, C. A., Veiga Júnior, J. P., Mendes, V. A., 2006. *Geologia e recursos minerais do estado do Rio Grande do Norte: texto explicativo dos mapas geológico e de recursos minerais do estado do Rio Grande do Norte escala 1:500.000*. CPRM - Serviço Geológico do Brasil, Recife, 119.

Araújo, M. G. S., Brito Neves, B. B., Archanjo, C., 2001. Idades $^{40}Ar/^{39}Ar$ do magmatismo básico Meso-Cenozóico da Província Borborema Oriental, nordeste do Brasil. *Boletim de Resumos, XIX Simpósio de Geologia do Nordeste*. SBG, Natal, 260–261.

Archanjo, C. J., Araújo, M. G. S., Launeau, P., 2002. Fabric of the Rio Ceará–Mirim mafic dike swarm (northeastern Brazil) determined by anisotropy of magnetic susceptibility and image analysis. *Journal of Geophysical Research: Solid Earth* **107**(B3). https://doi.org/10.1029/2001JB000268.

Arthaud, M. H., Caby, R., Fuck, R. A., Dantas, E. L., Parente, C. V., 2008. Geology of the northern Borborema Province, NE Brazil and its correlation with Nigeria, NW Africa. *Geological Society, London, Special Publications,* **294**(1): 49–67. https://doi.org/10.1144/SP294.4.

Baker, I., Haggerty, S. E., 1967., The alteration of olivine in basaltic and associated lavas: Part II: Intermediate and low temperature alteration. *Contributions to Mineralogy and Petrology*, **16**(3): 258–273. https://doi.org/10.1007/BF00371095.

Baldermann, A., Dohrmann, R., Kaufhold, S., Nickel, C., Letofsky-Papst, I., Dietzel, M., 2014. The Fe-Mg-saponite solid solution series – a hydrothermal synthesis study. *Clay Minerals*, **49**(3): 391–415. https://doi.org/10.1180/claymin.2014.049.3.04.

Barth-Wirsching, U., Hoeller, H., 1989. Experimental studies on zeolite formation conditions. *European Journal of Mineralogy*, **1**(4): 489–506.

Bastias, J., Fuentes, F., Aguirre, L., Hervé, F., Demant, A., Deckart, K., Torres, T., 2016. Very low-grade secondary minerals as indicators of palaeo-hydrothermal systems in the Upper Cretaceous volcanic succession of Hannah Point, Livingston Island, Antarctica. *Applied Clay Science*, **134**: 246–256. https://doi.org/10.1016/j.clay.2016.07.025.

Bellieni, G., Macedo, M. H. F., Petrini, R., Piccirillo, E. M., Cavazzini, G., Comin-Chiaramonti, P., Ernesto, M., Macedo, J. W. P., Martins, G., Melfi, A. J., Pacca, I. G., De Min, A., 1992. Evidence of magmatic activity related to Middle Jurassic and Lower Cretaceous rifting from northeastern Brazil (Ceará-Mirim): K/Ar age, palaeomagnetism, petrology and Sr/Nd isotope characteristics. *Chemical Geology*, **97**(1–2): 9–32. https://doi.org/10.1016/0009-2541(92)90133-P.

Bindeman, I. N., Greber, N. D., Melnik, O. E., Artyomova, A. S., Utkin, I. S., Karlstrom, L., Colón, D. P., 2020. Pervasive Hydrothermal Events Associated with Large Igneous Provinces Documented by the Columbia River Basaltic Province. *Scientific Reports*, **10**(1): 1–9. https://doi.org/10.1038/s41598-020-67226-9.

Birch, W. D., 1989. Chemistry of Victorian Zeolites. *In:* Birch, W. D. (Ed). *Zeolites of Victoria*. Mineralogical Society of Victoria, Melbourne, 91–102.

Caxito, F. D. A., Santos, L. C. M. D. L., Ganade, C. E., Bendaoud, A., Fettous, E.-H., Bouyo, M. H., 2020. Toward an integrated model of geological evolution for NE Brazil-NW Africa: The Borborema Province and its connections to the Trans-Saharan (Benino-Nigerian and Tuareg shields) and Central African orogens. *Brazilian Journal of Geology*, **50**(2): e20190122. https://doi.org/10.1590/2317-4889202020190122.

Chen, P.-Y., 1977. *Table of key lines in X-ray powder diffraction patterns of minerals in clays and associated rocks*. Department of Natural Resources, Bloomington, 67.

Chipera, S. J., Apps, J. A., 2001. Geochemical Stability of Natural Zeolites. *Reviews in Mineralogy and Geochemistry*, **45**(1): 117–161. https://doi.org/10.2138/rmg.2001.45.3.

Coombs, D. S., Alberti, A., Armbruster, T., Artioli, G., Colella, C., Galli, E., Grice, J. D., Liebau, F., Mandarino, J. A., Minato, H., Nickel, E. H., Passaglia, E., Peacor, D. R., Quartieri, S., Rinaldi, R., Ross, M., Sheppard, R. A., Tillmanns, E., Vezzalini, G., 1997. Recommended nomenclature for zeolite minerals: Report of the subcommittee on zeolites of the International Mineralogical Association, Commission on New Minerals and Mineral Names. *The Canadian Mineralogist*, **35**: 1571–1606.

Dainyak, L. G., Zviagina, B. B., Rusakov, V. S., Drits, V. A., 2006. Interpretation of the nontronite-dehydroxylate Mössbauer spectrum using EFG calculations. *European Journal of Mineralogy*, **18**(6): 753–764. https://doi.org/10.1127/0935?1221/2006/0018?0753.

Deer, W. A., Howie, R. A., Zussman, J., 2013. *An Introduction to the Rock-Forming Minerals*. 3rd Ed. The Mineralogical Society of Great Britain and Ireland, London, 498.

Duarte, L. C., Hartmann, L. A., Vasconcellos, M. A. Z., Medeiros, J. T. N., Theye, T., 2009. Epigenetic formation of amethyst-bearing geodes from Los Catalanes gemological district, Artigas, Uruguay, southern Paraná Magmatic Province. *Journal of Volcanology and Geothermal Research*, **184**(3–4): 427–436. https://doi.org/10.1016/j.jvolgeores.2009.05.019.

Eggleton, R. A., Foudoulis, C., Varkevisser, D., 1987. Weathering of Basalt: Changes in Rock Chemistry and Mineralogy. *Clays and Clay Minerals* **35**(3): 161–169. https://doi.org/10.1346/CCMN.1987.0350301.

Földvári, M., 2011. *Handbook of thermogravimetric system of minerals and its use in geological practice*. Geological Institute of Hungary, Budapest, 180.

Fridriksson, T., Bish, D. L., Bird, D. K., 2003., Hydrogen-bonded water in laumontite I: X-ray powder diffraction study of water site occupancy and structural changes in laumontite during room-temperature isothermal hydration/dehydration. *American Mineralogist*, **88**(2–3): 277–287. https://doi.org/10.2138/am-2003-2-304.

Galán, E., Ferrell, R. E., 2013. Genesis of Clay Minerals. *Developments in Clay Science*, **5**: 83–126.

Gatta, G. D., Cappelletti, P., Rotiroti, N., Slebodnick, C., Rinaldi, R., 2009. New insights into the crystal structure and crystal chemistry of the zeolite phillipsite. *American Mineralogist*, **94**(1): 190–199. https://doi.org/10.2138/am.2009.3032.

Gelves, J. F., Gallego, G. S., Marquez, M. A., 2016. Mineralogical characterization of zeolites present on basaltic rocks from Combia geological formation, La Pintada (Colombia). *Microporous and Mesoporous Materials*, **235**: 9–19. https://doi.org/10.1016/j.micromeso.2016.07.035.

Gislason, S. R., Arnórsson, S., 1993. Dissolution of primary basaltic minerals in natural waters: saturation state and kinetics. *Chemical Geology*, **105**(1–3): 117–135. https://doi.org/10.1016/0009-2541(93)90122-Y.

Gottardi, G., Galli, E., 1985. *Natural Zeolites*. Springer, Berlin, Heidelberg, 412.

Hartmann, L. A., Da Cunha Duarte, L., Massonne, H.-J., Michelin, C., Rosenstengel, L. M., Bergmann, M., Theye, T., Pertille, J., Arena, K. R., Duarte, S. K., Pinto, V. M., Barboza, E. G., Rosa, M. L. C. C., Wildner, W., 2012. Sequential opening and filling of cavities forming vesicles, amygdales and giant amethyst geodes in lavas from the southern Paraná volcanic province, Brazil and Uruguay. *International Geology Review*, **54**(1): 1–14. https://doi.org/10.1080/00206814.2010.496253.

Hassan, I. S., Al-Rashed, A. R., 2020. Zeolite-bearing amygdaloidal volcanic and volcanoclastic rocks at Gabal Katherine area, southern Sinai, Egypt. *Egyptian Journal of Geology*, **64**(1): 337–353. https://doi.org/10.21608/egjg.2020.216317.

Hollanda, M. H. B. M., Pimentel, M. M., Oliveira, D. C., De Sá, E. F. J., 2006. Lithosphere–asthenosphere interaction and the origin of Cretaceous tholeiitic magmatism in Northeastern Brazil: Sr–Nd–Pb isotopic evidence. *Lithos*, **86**(1–2): 34–49. https://doi.org/10.1016/j.lithos.2005.04.004.

Hollanda, M. H. B. M., Archanjo, C. J., Macedo Filho, A. A., Fossen, H., Ernst, R. E., De Castro, D. L., Melo, A. C., Oliveira, A. L., 2019. The Mesozoic Equatorial Atlantic Magmatic Province (EQUAMP): A New Large Igneous Province in South America. *In:* Srivastava, R. K., Ernst.

R. E., Peng, P. (Eds.), *Dyke Swarms of the World: A Modern Perspective*. Springer, Singapore, 87–110.

Honnorez, J., 1978. Generation of phillipsites by palagonitization of basaltic glass in seawater and the origin of K-rich deep-sea sediments. *In:* Sand, L. B., Mumpton, F. A. (Eds.), *Natural Zeolites - Occurrence, Properties, Use.* Pergamon Press, Oxford, 245–258.

Irvine, T. N., Baragar, W. R. A., 1971. A Guide to the Chemical Classification of the Common Volcanic Rocks. *Canadian Journal of Earth Sciences*, **8**(5): 523–548. https://doi.org/10.1139/e71-055.

Jeong, G. Y., Sohn, Y. K., 2011. Mineralogy and Microtextures of Basaltic Glass Alteration in Hyaloclastite, Jeju Island, Korea. *Journal of Analytical Science-Technology*, **2**(1): 177–186.

Kónya, P., Szakáll, S., 2011. Occurrence, composition and paragenesis of the zeolites and associated minerals in the alkaline basalt of a maar-type volcano at Haláp Hill, Balaton Highland, Hungary. *Mineralogical Magazine*, **75**(6): 2869–2885. https://doi.org/10.1180/minmag.2011.075.6.2869.

Kousehlar, M., Weisenberger, T. B., Tutti, F., Mirnejad, H., 2012. Fluid control on low-temperature mineral formation in volcanic rocks of Kahrizak, Iran. *Geofluids*, **12**(4): 295–311. https://doi.org/10.1111/gfl.12001.

Kristmannsdóttir, H., 1979. Alteration of Basaltic Rocks by Hydrothermal-Activity at 100-300°C. *Developments in Sedimentology*, **27**: 359–367. https://doi.org/10.1016/S0070-4571(08)70732-5.

Kristmannsdóttir, H., Tomasson, J., 1978. Zeolite zones in geothermal areas in Iceland. *In:* Sand, L. B., Mumpton, F. A. (Eds.), *Natural Zeolites - Occurrence, Properties, Use*. Pergamon Press, Oxford, 277–284.

Krogh Andersen, E., Krogh Andersen, I. G., Ploug-Sorensen, G., 1990. Disorder in natrolites; structure determinations of three disordered natrolites and one lithium-exchanged disordered natrolite. *European Journal of Mineralogy*, **2**(6): 799–807.

Kusehlar, M., Tutti, F., Mirnejad, H., Lalonde, A. E., 2010. Mineralogical characterization of fibrous zeolites from the Kahrizak volcanic suite, south Tehran, Iran. *Clay Minerals*, **45**(4): 507–517. https://doi.org/10.1180/claymin.2010.045.4.507.

Larsen, G., Plum, K. H., Foerster, H., 1991. Zeolites and other hydrothermal alteration products of synthetic glasses. *European Journal of Mineralogy*, **3**(6): 933–941.

Le Bas, M. J., Le Maitre, R. W., Streckeisen, A., Zanettin, B., IUGS Subcommission on the Systematics of Igneous Rocks., 1986. Chemical classification of volcanic rocks based on the total alkali–silica diagram. *Journal of Petrology*, **27**(3): 745–750. https://doi.org/10.1093/petrology/27.3.745.

Lee, Y., Vogt, T., Hriljac, J. A., 2004. Pressure-induced migration of zeolitic water in laumontite. *Physics and Chemistry of Minerals*, **31**(7). https://doi.org/10.1007/s00269-004-0414-y.

Liou, J. G., De Capitani, C., Frey, M., 1991. Zeolite equilibria in the system $CaAl_2Si_2O_8$-$NaAlSi_3O_8$-SiO_2-H_2O. *New Zealand Journal of Geology and Geophysics*, **34**(3): 293–301.

Macêdo Filho, A. A., Oliveira, A. L., Klöcking, M., Janasi, V. A., Archanjo, C. J., Lino, L. M., 2025. Petrology of Cenomanian basalts on the Brazilian equatorial margin: Implications for the tectonomagmatic evolution of the drift phase. *Geochemistry*, **85(1)**: 126248. https://doi.org/10.1016/j.chemer.2025.126248.

Markússon, S. H., Stefánsson, A., 2011. Geothermal surface alteration of basalts, Krýsuvík Iceland—Alteration mineralogy, water chemistry and the effects of acid supply on the alteration process. *Journal of Volcanology and Geothermal Research*, **206**(1–2): 46–59. https://doi.org/10.1016/j.jvolgeores.2011.05.007.

Mattioli, M., Cenni, M., Passaglia, E., 2016. Secondary mineral assemblages as indicators of multistage alteration processes in basaltic lava flows: evidence from the Lessini Mountains, Veneto Volcanic Province, Northern Italy. *Periodico di Mineralogia*, **85**: 1–24. https://doi.org/10.2451/2015PM0375.

Mizusaki, A. M. P., Thomaz-Filho, A., Milani, E. J., De Césero, P., 2002. Mesozoic and Cenozoic igneous activity and its tectonic control in northeastern Brazil. *Journal of South American Earth Sciences*, **15**(2): 183–198. https://doi.org/10.1016/S0895-9811(02)00014-7.

Moore, G., Carmichael, I., 1998. The hydrous phase equilibria (to 3 kbar) of an andesite and basaltic andesite from western Mexico: constraints on water content and conditions of phenocryst growth. *Contributions to Mineralogy and Petrology*, **130**: 304–319. https://doi.org/10.1007/s004100050367.

Nemecz, E., 1981. *Clay minerals*. Akadémiai Kiadó, Budapest, 547.

Neuhoff, P. S., 1999. Porosity evolution and mineral paragenesis during low-grade metamorphism of basaltic lavas at Teigarhorn, eastern Iceland. *American Journal of Science*, **299**(6): 467–501. https://doi.org/10.2475/ajs.299.6.467.

Neves, S. P., Tommasi, A., Vauchez, A., Carrino, T. A., 2021. The Borborema Strike-Slip Shear Zone System (NE Brazil): Large-Scale Intracontinental Strain Localization in a Heterogeneous Plate. *Lithosphere*, **2021**(Special 6): 6407232. https://doi.org/10.2113/2021/6407232.

Ngonge, E. D., De Hollanda, M. H. B. M., Archanjo, C. J., De Oliveira, D. C., Vasconcelos, P. M. P., Muñoz, P. R. M., 2016. Petrology of continental tholeiitic magmas forming a 350-km-long Mesozoic dyke swarm in NE Brazil: Constraints of geochemical and isotopic data. *Lithos*, **258–259**: 228–252. https://doi.org/10.1016/j.lithos.2016.04.008.

Ottens, B., Götze, J., Schuster, R., Krenn, K., Hauzenberger, C., Zsolt, B., Vennemann, T., 2019. Exceptional multistage mineralization of secondary minerals in cavities of flood basalts from the deccan volcanic province, India. *Minerals*, **9**(6). https://doi.org/10.3390/min9060351.

Özen, S., Göncüoğlu, M. C., 2015. Sequential Formation of Natrolite-Group Zeolites In Amygdules of Basaltic Lavas. *The Canadian Mineralogist*, **53**(4): 757–765. https://doi.org/10.3749/canmin.1500036.

Passaglia, E., 1970. The crystal chemistry of chabazites. *American Mineralogist*, **55**(7–8): 1278–1301.

Pe-Piper, G., Miller, L., 2003. Zeolite minerals from the North Shore of the Minas Basin, Nova Scotia. *Atlantic Geology*, **38**(1): 11–28. https://doi.org/10.4138/1252.

Pichavant, M., Macdonald, R., 2007. Crystallization of primitive basaltic magmas at crustal pressures and genesis of the calc-alkaline igneous suite: experimental evidence from St Vincent, Lesser Antilles arc. *Contributions to Mineralogy and Petrology*, **154**: 535–558. https://doi.org/10.1007/s00410-007-0208-6.

Robert, C., 2001. Hydrothermal alteration processes of the Tertiary lavas of Northern Ireland. *Mineralogical Magazine*, **65**(4): 543–554. https://doi.org/10.1180/002646101750377560.

Senderov, E. E., 1988. Physical-chemical aspects of zeolite formation in nature. in: Occurrence, Properties and Utilization of Natural Zeolites. *In:* Kalló D., Sherry H. S. (Eds.), *Occurrence, Properties and Utilization of Natural Zeolites*. Akadémiai Kiadó, Budapest, 111–147.

Seyfried, W. E., Bischoff, J. L., 1979. Low temperature basalt alteration by sea water: an experimental study at 70 °C and 150 °C. *Geochimica et Cosmochimica Acta*, **43**(12): 1937–1947. https://doi.org/10.1016/0016-7037(79)90006-1.

Sial, A. N., 1978. Major and trace chemistry of the Tertiary basaltic suite of Rio Grande do Norte and Paraíba, northeast Brazil. *Jornal de Mineralogia*, **7**: 119–128.

Sisson, T. W., Grove, T. L., 1993. Temperatures and H_2O contents of low-MgO high-alumina basalts. *Contributions to Mineralogy and Petrology*, **113**: 167–184. https://doi.org/10.1007/BF00283226.

Souza, Z. S., Vasconcelos, P. M., Nascimento, M. A. L., Silveira, F. V., Dias, L. G. S., Thiede, D., Carmo, I. O., 2003. $^{40}Ar/^{39}Ar$ Geochronology of Mesozoic and Cenozoic Magmatism in Ne Brazil. *In: Short Papers - IV South American Symposium on Isotope Geology*. CBPM, Salvador, Brazil. 691-694.

Souza, Z. S., Kalsbeek, F., Deng, X.-D., Frei, R., Kokfelt, T. F., Dantas, E. L., Li, J.-W., Pimentel, M. M., Galindo, A. C., 2016. Generation of continental crust in the northern part of the Borborema Province, northeastern Brazil, from Archaean to Neoproterozoic. *Journal of South American Earth Sciences*, **68**: 68–96. https://doi.org/10.1016/j.jsames.2015.10.006.

Stefánsson, A., Gislason, S. R., 2001. Chemical weathering of basalts, southwest Iceland: effect of rock crystallinity and secondary minerals on chemical fluxes to the ocean. *American Journal of Science*, **301**(6): 513–556. https://doi.org/10.2475/ajs.301.6.513.

Stuckenschmidt, E., Joswig, W., Baur, W. H., 1996. Flexibility and distortion of the collapsible framework of NAT topology: the crystal structure of H_3O-natrolite. *European Journal of Mineralogy*, **8**(1): 85–92. https://doi.org/10.1127/ejm/8/1/0085.

Triana, J. M. R., Herrera, J. F. R., Ríos, C. A. R., Castellanos, O. M. A., Henao, J. A. M., Williams, C. D., Roberts, C. L., 2012. Natural zeolites

filling amygdales and veins in basalts from the British Tertiary Igneous Province on the Isle of Skye, Scotland. *Earth Sciences Research Journal*, **16**(1): 41–53.

Van Schmus, W. R., Oliveira, E. P., Silva Filho, A. F., Toteu, S. F., Penaye, J., Guimarães, I. P., 2008. Proterozoic links between the Borborema Province, NE Brazil, and the Central African Fold Belt. *Geological Society, London, Special Publications*, **294**(1): 69–99. https://doi.org/10.1144/SP294.5.

Vauchez, A., Neves, S., Caby, R., Corsini, M., Egydio-Silva, M., Arthaud, M., Amaro, V. E., 1995. The Borborema shear zone system, NE Brazil. *Journal of South American Earth Sciences*, **8**(3–4): 247–266. https://doi.org/10.1016/0895-9811(95)00012-5.

Verati, C., Jourdan, F., 2014. Modelling effect of sericitization of plagioclase on the $^{40}K/^{40}Ar$ and $^{40}Ar/^{39}Ar$ chronometers: implication for dating basaltic rocks and mineral deposits. *Geological Society, London, Special Publications*, **378**(1): 155–174. https://doi.org/10.1144/SP378.14.

Walker, G. P. L., 1960. The amygdale minerals in the Tertiary lavas of Ireland. III. Regional distribution. *Mineralogical Magazine and Journal of the Mineralogical Society*, **32**(250): 503–527. https://doi.org/10.1180/minmag.1960.032.250.01.